2 State of the art

Materials processing with lasers is an emerging field, within which a variety of laser processing techniques such as cutting, drilling, welding, piercing, patterning, rapid prototyping, macro- and micromachining, forming, cleaning and using lasers in biomedical processes have been established [Steen2010]. Laser processing of materials usually takes place in ambient air, thus using laser intensities that remove material from a workpiece's surface and the particles are released into the environment. These particles generated by laser irradiation are in the size regime of nanometers [Ullmann2002]. If these particles are released into ambient air, they bare the risk of adverse health effects when inhaled [Barcikowski2009a]. An alternative approach whereby particles are released yet captured is through laser materials processing in liquids [Fojtik1993]. After removal from the material's surface, the particles are confined in the liquid, thus avoiding their release into the workplace. This technique has been established in recent decades for nanoparticle generation, where it is not the processed workpiece that holds interest but rather the produced particles. A modification of this pulsed laser ablation in liquids (PLAL) technique is the laser irradiation of particles in the micro, sub-micro or nano range [Fojtik1993]. In contrast to PLAL, pulsed laser fragmentation in liquids (PLFL) is less intensely studied, resulting in the lack of mechanistic understanding and an awareness of the possibilities that this processing technique offers, which motivates this dissertation.

Chapters 2.1 and 2.2 will introduce to the materials selected as model materials for the practical part of this work, representing a semiconductor and metal material, respectively. Furthermore, an introduction is provided into the current state of the art to the interaction of particles with intense laser light in chapter 2.3, before the fundamental aspects of PLFL and PLML are explained (chapter 2.5 and 2.6). This will lead to the novel experimental set-up, which is developed and exploited, whereby an insight is provided into the possibilities that arise from the developed set-up. With this design, particle properties and laser parameters can be correlated and basic mechanistic conclusions of PLFL can be drawn. It will also be shown that for controlling PLFL, it is necessary to control the adapted laser

M. Lau, *Laser Fragmentation and Melting of Particles*,
MatWerk, DOI 10.1007/978-3-658-14171-4_2

fluence as precisely as possible. Furthermore, the developed set-up enables determining the specific energy input converted into particle properties.

2.1 Zinc oxide

Zinc oxide is commonly used as a color pigment, e.g. in paints [Wöll2007]. Moreover, it is also a semiconductor with a direct band gap of around 3.3 eV, a density of 5.61 g/cm³, a Mohs hardness of around 4.5 [Hernández Battez2008] and a wurtzite crystal lattice structure. It occurs rarely in nature and deposits can be found as zincite. After chemical synthesis, it forms a white powder. Özgür and Morkoç et al. reviewed the properties of zinc oxides and described pure zinc oxide, effects of doping and the variety of fabrication methods and application fields such as light-emitting devices, UV lasing, photodiodes, transparent conductive oxides (TCO), thin film transistors, piezoelectric devices, solar cells, gas sensors and bio sensors [Özgür2005], [Morkoç2008]. For several of these applications, engineering of the bandgap plays an important role in controlling and changing the electronic and photonic properties. Oba et al. showed that defects in the wurtzite ZnO lattice cause a change in the energy levels between the conductive and valence band [Oba2008]. Janotti et al. reviewed the possibilities of band gap engineering and effects of defects in zinc oxide, showing that n-type conductivity is promising for several applications [Janotti2008]. Dorranian et al. described photoluminescence of ZnO nanoparticles fabricated by PLAL from a Zn metal target in a water environment [Dorranian2012] attempting to correlate the photoluminescence properties to the applied wavelengths and fluences. Although they postulated an energy level scheme for the different possible transitions in the ZnO lattice, they could not clearly correlate generated particle properties with the laser parameters used for particle generation. Jadraque et al. showed the creation of oxygen vacancies on ZnO targets irradiated with different UV laser wavelengths under vacuum conditions [Jadraque2008]. For this, a 308 nm laser wavelength was more efficient to induce these defects compared to 266 nm. This shows that bandgap engineering and control of zinc oxide properties is a relevant research field due to the potential in application of different modifications from zinc oxide, such as TCO [Janotti2008]. Owing to the comparably low price and basic availability, it is a potential substitute for ITO [Ellmer2011]. Hiramatsu et al. showed that highly conductive TCO films can be generated by laser ablation of target materials in gas phase and

a subsequent deposition onto a substrate [Hiramatsu1998]. They ablated target materials prepared from zinc oxide powders containing germanium oxide or aluminum oxide powders, known to be an effective dopant for this purpose [Luo2013]. For this, the powders were mixed and sintered prior to laser ablation, which resulted in a highly conductive TCO onto the substrate, comprising the comparably cheap educts such as ZnO and Al_2O_3 powders. Usui et al. reported about the laser ablation of a zinc plate and obtained zinc oxide nanoparticles [Usui2005], thus showing the (partial) oxidation of the material. Nonetheless, a comprehensive understanding is lacking [Avadhut2012], [Ciupina2004], [Yang2012], [Rajeswari2011], [Kelchtermans2013].

Further engineering of zinc oxides bandgap is a promising method to modify the material. This holds particular interest as zinc oxide and defect-rich zinc oxide particles are promising, e.g. for catalytic applications [Wöll2007]. Lin et al. determined green emission from oxide antisite defect rather than a crystallographic vacancy or interstitial [Lin2001]. They proposed the scheme in Figure 1 for energy levels [Lin2001], whereby this band gap (E_g) results in a local peak around 370 nm for ZnO nanoparticle dispersions in the UV-vis extinction spectrum [Srikant1998], [Zak2011].

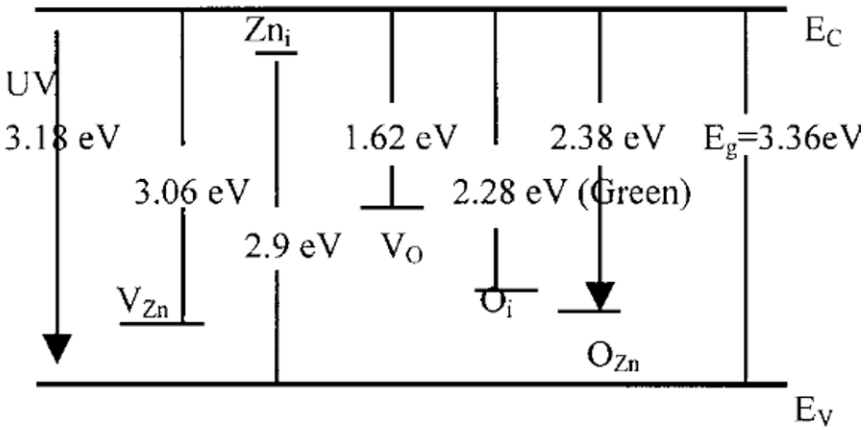

Figure 1: Scheme of energy levels with energy levels of conduction band (E_C), valence band (E_V), zinc vacancy (V_{Zn}), interstitial zinc (Zn_i), oxygen vacancy (V_O), interstitial oxygen (O_i) and oxygen antisite defect (O_{Zn}) (taken with permission from Lin et al. [Lin2001])

For processing of zinc oxide particles in liquid environment, its solubility also needs to be considered. Schindler et al. reported about the free enthalpy of formation [Schindler1964] and solubility in water in dependence of zinc oxide's particle size [Schindler1965]. Besides, ZnO, $Zn(OH)_2$, α-$Zn(OH)_2$, β_1-$Zn(OH)_2$, β_1-$Zn(OH)_2$, γ-$Zn(OH)_2$, δ-$Zn(OH)_2$, and ε-$Zn(OH)_2$ can occur as solid states in a liquid environment [Schindler1964].

Schindler et al. also proposed the following equation for zinc oxides solubility in dependence of the particle diameter [Schindler1965]:

$$\log Ks_0 = -16(\pm 0.05) + \frac{50(\pm 26)}{d_p \cdot 10}$$

With Ks_0: solubility product, d_p: particle diameter in nm

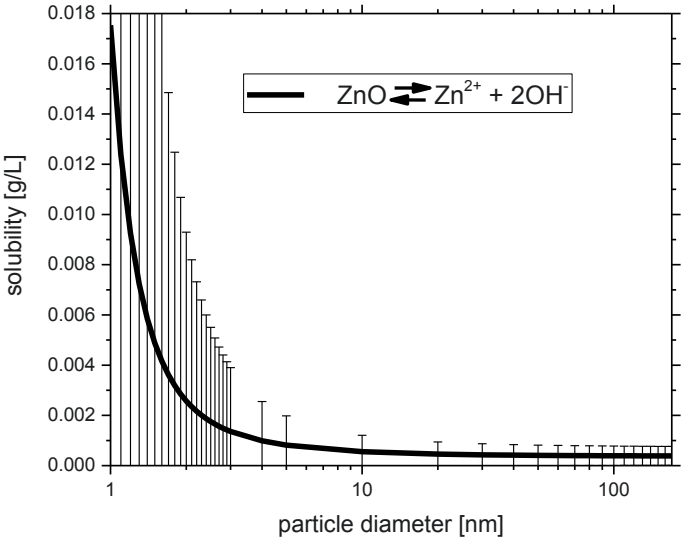

Figure 2: Calculated solubility of ZnO in water at a pH of 6.7 in dependence of the particle diameter [Schindler1965]

Figure 2 shows a diagram for the solubility plotted versus the particle diameter using the equation of Schindler et al. with the corresponding equation for dissolution of ZnO in water environment. For particle diameters below 5 nm, this solubility significantly increases but does not exceed 18 mg/L for 1 nm particles. Note that the error bars are larger; thus, the solubility of such small particles might be higher.

The solubility of ZnO powder from the GESTRIS data base is given with 1.6 mg/L, meaning that zinc oxide is almost not soluble in water.

To summarize, it can be stated that zinc oxide is promising for several applications besides its use as a white pigment in simple paints, due to the manifold electronic structure [Lin2001]. Thus, it can be used, in catalysis [Wöll2007] or as varistors in electronic devices [Gupta1990], for instance. Several potential applications arise when it is in the nanoscale [Wang2004], such as a nanolasing device [Huang2001].

Accordingly a method to modify zinc oxides electronic structure and size by a precisely controlled process might be promising.

2.2 Gold nanoparticles

Gold nanoparticles (Au NP) hold particular interest in a variety of fields such as catalysis [Hartua1997], as well as biology and medicine [Giljohann2010], [Murphy2008]. The possible application fields and different synthesis strategies have been studied intensely over many decades [Daniel2004]. Due to their optical properties which differ from the bulk material and are size- and shape-dependent the interest in Au NP ranges from fundamental research to real-world applications. The discovery of deviation of optical properties for gold nanoparticles compared to the bulk material dates back to Faraday in 1857 [Faraday1857].

Many chemical bottom-up synthesis routes exist for the fabrication of gold nanoparticles, whereas only a few top-down methods provide access to Au NP. One of the most common synthesis routes for gold nanoparticles was reported by Turkevich in 1951 [Turkevich1951]. Another popular bottom-up synthesis is the Brust-Shiffrin method [Brust1994]. Turkevich's citrate-based method delivers

particle sizes between 10-25 nm that show good colloidal stability in water. The advantage of Brust's method to obtain comparably small particle sizes and widths of particle size distributions is accompanied by the drawback that the thiols used for size quenching strongly bind to particles' surface [Häkkinen2012], [Xue2014], thus making a subsequent ligand exchange or removal difficult. Overall, a variety of synthesis routes and potential applications are discussed and shown, although for some applications (e.g. biological, catalytic) impurities like residual chemicals or abrasion from comminution processes are an immense problem [Goesmann2010], [Raab2011]; thus, subsequent cleaning steps are required.

A real-world application in which purity and size plays an important role is the use of gold nanoparticles in catalysis [Haruta1997]. Masatake Haruta first showed the activity of gold nanoparticles in catalysis and its size dependency on the activity [Haruta1987], [Haruta1997]. For catalytic applications, small particles are preferential. Activity of gold nanoparticles in catalysis is correlated to the free surface and significant increase in activity can be observed below 5 nm [Haruta1997]. As support particles for gold nanoparticles, titanium dioxide is used, e.g. for oxidation of CO (water-gas shift reactions) [Sakurai1997].

Here, the laser generation of gold nanoparticles comes into play, which can deliver pure and ligand-free gold nanoparticles harvested in a liquid environment. A synthesis method bypassing the drawback of a ligand-occupied surface is laser ablation in liquids. First reported by Fojtik and Henglein [Fojtik1993], this method has gained increasing interest as many efforts in up-scaling and process control have been established in the last decade. The PLAL technique fabricates ligand-free gold nanoparticles from a plasma plume, which is followed by cavitation bubbles directly from the bulk material [Ibrahimkutty2012]. Besides the expansion and collapse of one first major cavitation bubble which is followed by smaller ones that expand and collapse on the target's surface it could be shown that primary particles in the size range of around 7 nm can pass the phase boundary, whereas larger aggregates and agglomerates with 40-60 nm are kept in the bubble [Wagener2013]. The detailed small angle X-ray scattering experiments by Wagener et al. provided an insight into what happens inside the cavitation bubble and where and when particles are formed. Beside this, there are also investigations and evidence of metal atom clusters formed after PLAL [Giorgetti2014]; nonetheless, PLAL generally delivers a wide particle size distribution. Recently Rehbock et al. reviewed how monodisperse and ligand-free gold nanoparticles can be obtained by PLAL [Rehbock2014].

Due to the possibilities in manufacturing ligand-free particles by PLAL e.g. freedom of material and solvent [Baersch2009], embedding them into polymers for biological applications [Hahn2010], [Sowa-Soehle2013] or supporting the nanoparticles to microparticle supports [Wagener2012a] this technique has attracted increasing interest and use [Barcikowski2009], [Asahi2015].

Given that catalysis application requires free surfaces and small particle diameter, ultra-small ligand-free particles would be desirable. However, unfortunately to prevent these small gold nanoparticles from growing when they are synthesized e.g. by chemical reduction strong binding organic ligands are necessary [Schmid1981], [Schmid2008]. These ligands enable precise control of ultra-small gold particle sizes but simultaneously cover the surface.

The size limit for laser-generated and ligand-free gold nanoparticles is reported at around 4 nm in diameter [Amendola2007], [Rehbock2014], although smaller ligand-free nanoparticles would be desired due to higher specific surface area and probably high reactivity.

2.3 Different lasers for one application – particle processing

Since the first report of light amplification by stimulated emission of radiation (laser) in ruby by Maiman [Maiman1960a], [Maiman1960b], [Maiman1962] many efforts and developments have been engaged in manufacturing lasers with higher intensity. The following figure depicts the development of the available focused laser intensity versus time (left) and the peak power plotted versus the average power for different femtosecond systems (right) [Sibbett2012]. The diagram from Sibbett et al. also indicates the average and peak power demanded for different applications such as biomedicine, telecommunications and materials processing, highest demands in average power and pulse peak power are found for materials processing, including laser ablation.

At present, these high intensities are only achieved by pulsing of the laser. The duration of a single released pulse (pulse length) has a crucial impact on the response of the processed material regarding short (nanoseconds) and ultra-short (starting from femtoseconds to a few picoseconds) pulsed lasers, owing to the relaxation time of electrons releasing their energy to the lattice structure of atoms in solids in the range of picoseconds [Chichkov1996]. Due to this relaxation

time, materials processing with picosecond lasers can be regarded as cold processes, whereas nanosecond materials processing will cause significant thermal effects to the material. In this work, all thresholds are described as fluence at fixed pulse duration defined as the energy of a single pulse divided by the area excited by focusing the laser beam. However, these thresholds only hold for the applied pulse length. Therefore, laser fragmentation with picosecond pulses will have lower fragmentation threshold fluences compared to nanosecond pulses, although the energy dose put into a particle is the same, owing to the aforementioned relaxation time of electrons.

It could be estimated that dividing the pulse energy by its duration (pulse length) will give an intensity threshold for material processing (depending on the optical material properties) that is independent on pulse length. However, due to the difference in mechanisms occurring for different pulse length for material processing, a uniform fragmentation (or ablation) threshold with the unit "intensity per pulse" which is independent of the pulse length will not exist. Nonetheless, as the mechanism occurring for material ablation or disruption can be correlated to the electron-phonon coupling time, there should be a possible differentiation in case of undergoing this electron-phonon coupling time and for sufficient time for electron relaxation (heating of the material). Lin and Zhigilei reported this time for Au in the range of 6 ps to 20 ps [Lin2003] and for ZnO this value is reported to be around 500 fs, thus half a picosecond [Zhukov2012]. This means that for ZnO including the case of the 10 ps used within the experiments there is sufficient time to cause thermal effects. However, for Au, the transition regime is addressed with 10 ps, which might make thermal effects e.g. melting or heating-evaporation more difficult compared to ZnO.

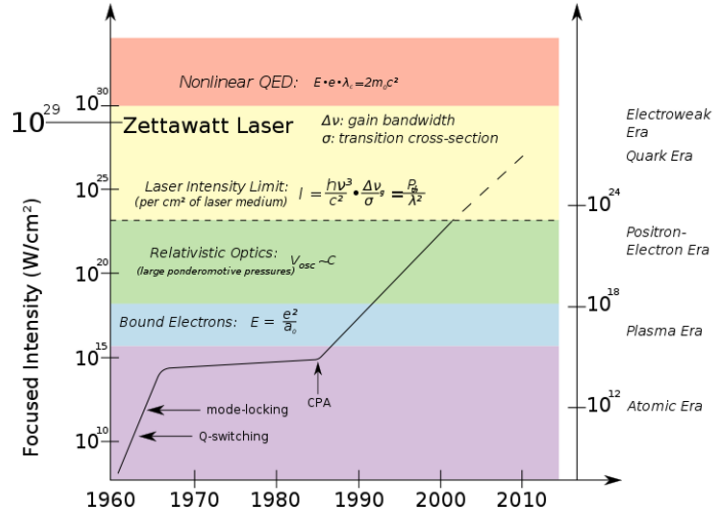

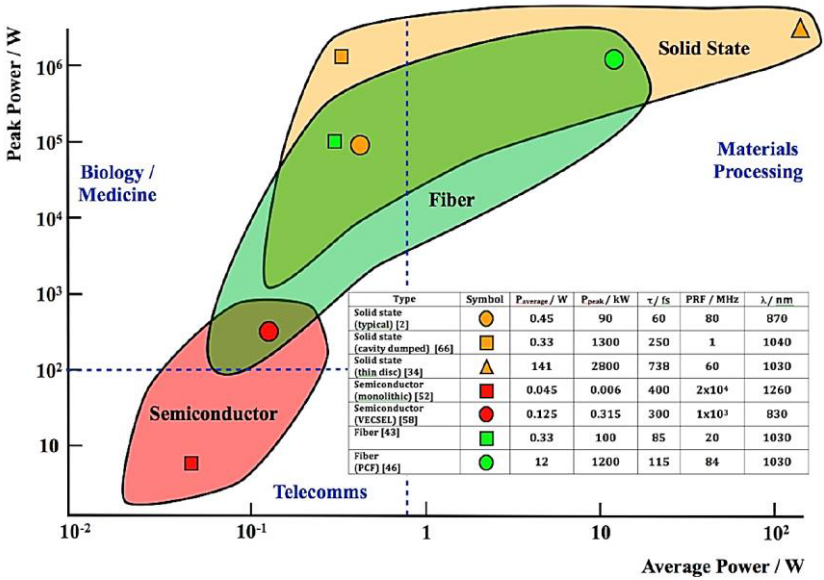

Figure 3: Development of available focused laser intensity over time [published work into the public domain at wikimedia commons, Wikipedia 03/21/2015] (top) and peak power versus the average power for different femtosecond systems taken with permission from Sibbett et al. [Sibbett2012] (bottom)

2.4 Interaction of light with particles

Light scattering

Light scattering of particles in particular small particles is a phenomenon that has long fascinated scientists. John Tyndall described general scattering observations of condensed light from an electrical lamp scattered by vapor in a glass tube. Inspired by Sir John Herschel and with suggestions of a refined experiment from Prof. George Gabriel Stokes, John Tyndall found the formation of a "blue cloud" in the glass tube [Tyndall1869]. Through observation from different angles during his experiment, he provided the first explanation for the blue appearance of a cloud-free sky, the scattering of light on small particles. Furthermore, he even stated the polarization of light when scattered on such small particles. Although he also mentioned a dependence of the particle size on this scattering effect, it was Gustav Mie who described this effect in detail by solving Maxwell's equations [Mie1908]. The Mie-Theory holds well for particles with diameters of 2-10 times λ, whereby λ is the wavelength of the light.

John William Strutt, 3rd Baron Rayleigh described the blue appearance of the sky and sea from particles smaller than 0.2 λ and thus this effect is known as Rayleigh-scattering [Rayleigh1910], although the meteorologist John Aitken had previously described the same phenomenon [Aitken1881]. John Aitken found that "extremely small particles of matter suspended in water" [Aitken1881] only scatter the short wavelengths of the light (although Rayleigh first described the size dependency mathematically). From his experiments, he proved that the hitherto-named, "selective scattering theory" holds rather than the "selective absorption theory" [Aitken1881]. The former stated that scattering of the blue region of light waves is responsible for the bluish sea color and the latter that selective absorption of the red color region is responsible for this appearance. This shows that even over one hundred years ago, scientists were familiar with the different possibilities of light and matter interaction and the dependence of the light wavelengths. Indeed, even nowadays, the optical appearance of the sky remains a relevant research topic [Gedzelman2005]. Rayleigh found that the intensity of scattering is proportional to the volume of a particle and proportional to λ^{-4} of the incident light wavelength [Rayleigh1899].

A drawback during the experimental observations during that time was that no monochromatic light source was available. Owing to the dependence of the incident angle of light and the wavelength of the light on the scattering effect on

a particle with a defined size, a monochromatic light source with parallel beam with no or low divergence would be favorable. Thus, the discovery of light amplification by stimulated emission of radiation (LASER) was beneficial for further investigations [Maiman1960a], [Maiman1960b]. In particular, the availability of increasingly higher laser energies offers new possibilities in particle excitation.

Light absorption

The portion of light that is neither scattered nor transmitted through the particle is absorbed. Sufficient and fast excitation results in the formation of electron hole pairs within a few femtoseconds [Amendola2008]. These are transferred into hot electrons during a few hundreds of femtoseconds. Based upon the two temperature model, energy or heat is transferred to the atom lattice within a few picoseconds [Chichkov1996]. As a result, the excited electrons transfer energy in the form of heating of the atomic lattice occurs within a few picoseconds, e.g. for gold [Lin2003], [Werner2011a]. Note that if energy input is caused with ultra-short pulses fragmentation mechanisms will differ, whereby a so-called coulomb explosion is known to cause a cold ablation of material [Chichkov1996].

Subsequently, energy transfer from electrons to atoms causes heating of the particle. The resulting temperature can be determined from the energy portion transferred into the particle although the temperature dependency of the specific heat capacity should be considered [Furukawa1968]. If a solid particle in liquid environment heats up, four temperature regimes should be distinguished. If the time of particle heating is much shorter than the time required for sufficient heat transfer (from heated particle to the surrounding medium), it is possible that a liquid or vaporized particle is directly surrounded by the liquid medium for a short period of time. As a result, the molten or vaporized material can dissolve (e.g. as ions or atoms) directly in the liquid environment if soluble in the present concentration. For sufficient heat transfer, the system can undergo the following stages during particle heating and energy transfer to its liquid environment: solid particle surrounded by liquid, solid particle surrounded by gas, liquid particle surrounded by gas, vaporized particle surrounded by gas. Considering the possibility of a shock wave-induced particle fragmentation [Zhigilei1998], the possible stages shown in Figure 3 might occur after intense laser light absorption for a single particle.

This holds particular interest as this work addresses the intense irradiation with pico- and nanosecond laser sources. Figure 3 sketches the possible excitation and

relaxation stages based upon literature and own findings. Vaporization [Schaumberg2014], bubble formation [Hashimoto2012], shock wave-induced fragmentation [Zhigilei1998] and particle melting [Link1999a] are known particle responses to intense photonic excitation.

After sufficient laser pulse absorption (see Figure 3 top) three different time regimes can be distinguished. For τ_P (duration of a single pulse) >> $\tau_{e\text{-}p}$ (material specific electron-phonon coupling time), electrons have sufficient time to transfer the energy received from laser irradiation (phonons) to the atomic lattice. Thus, they can transfer the energy resulting in heating, melting and vaporization of the particle for sufficient energy input. These stages potentially occurring for $\tau_P >> \tau_{e\text{-}p}$ in chronological order (from top to bottom) are shown in the left column of Figure 3 [Link1999a], [Hashimoto2012], [Schaumberg2014].

For $\tau_P \approx \tau_{e\text{-}p}$, it might be estimated that both effects can occur, namely the mechanism of shock wave-driven particle fragmentation and heating-melting-evaporation. The electron-phonon coupling times for zinc oxide (around 0.5 ps) [Zhukov2012] and gold (around 6 to 20 ps) [Lin2003] fall in the range of 1-10 ps lasers. As $\tau_{e\text{-}p}$ time for Au is longer than $\tau_{e\text{-}p}$ time for ZnO, it might be estimated that with 10 ps laser pulses ZnO might be more effectively heat affected [Lau2014a]. This is schematically illustrated in the center column of Figure 3.

A distinctive shock wave-driven fragmentation mechanism might be assumed for $\tau_P << \tau_{e\text{-}p}$ [Zhigiliei1998]. If the laser pulse duration is distinctively lower that the material dependent $\tau_{e\text{-}p}$, electrons can be sufficiently excited to cause a coulomb explosion of the material without being heat affected [Chichkov1996]. This is illustrated in the column on the right of Figure 3.

Note that these are only suggested relaxation routes based upon the reported observations and theory from literature, although this is in agreement considering the electron-phonon coupling times for zinc oxide [Zhukov2012], and with own experimental findings as will be shown later.

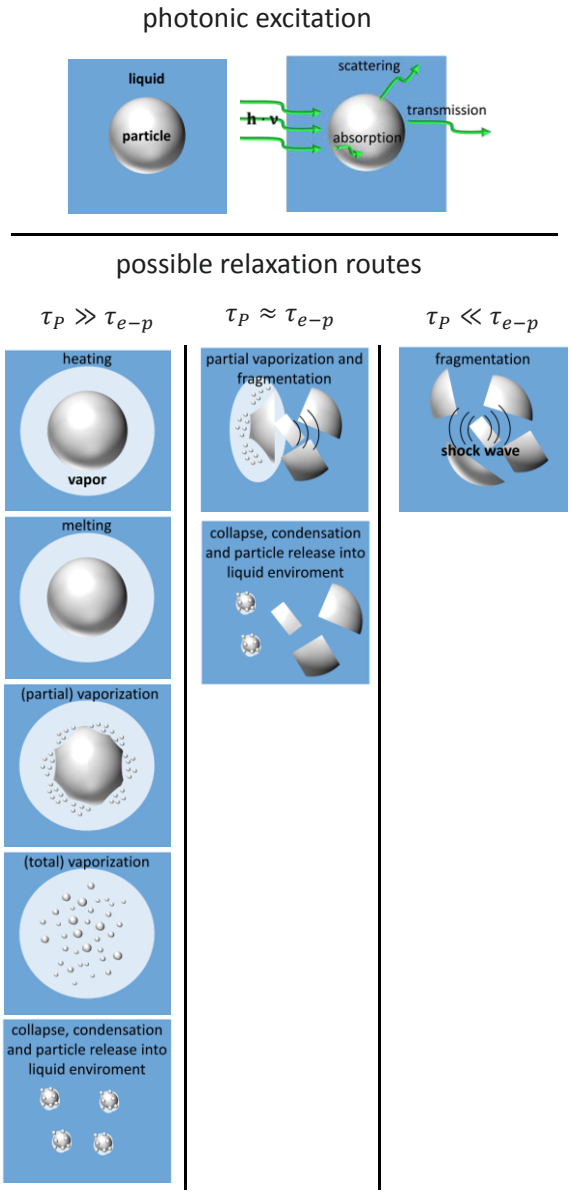

Figure 4: Proposed possible relaxation routes of a small particle after intense laser light absorption

2.5 Fundamentals of laser fragmentation

Intense laser light excitation of particles suspended in liquids enables their modification in structure and size. If the target particles are irradiated with a sufficient energy dose, their size can decrease by one of the pathways described in chapter 2.4, resulting in the formation of nanoparticles. This fabrication method of nanoparticles from suspended micro- or nanoparticles is mostly described as laser fragmentation. Besides the term “laser fragmentation”, “laser ablation (of particles)” [Schaumberg2014], [Jeon2007], [Asahi2008] or “(post)- irradiation” (“post-” in case of irradiation of previously fabricated nanoparticles by PLAL) [Amendola2007], [Zhang2003] can be found in literature, although these terms usually do not match the mechanisms that occur. The term laser ablation (of particles) results from a problem that invariably arises for all particle size reduction techniques. For all comminution processes, the particle size distribution changes and this is usually associated with an educt-product particle mixing. Thus, investigation of the smallest fraction after laser fragmentation is most convenient, because the nanoparticles can be extracted from educt particles by sedimentation of the educt (micro-) particles. However, an analysis of the whole particle fractions would allow better understanding the PLFL process.

This work will show that PLFL can follow two major mechanisms, namely shock wave-induced particle disruption and nanoparticle generation by vaporization. The size difference between the educt MP and the NP fabricated by vaporization enables the separation of these two fractions. As a result, some researchers name this process laser ablation of MPs, neglecting the shock wave-induced particle fragmentation. Therefore, they do not consider all fragments of particles that are generated, such as shock wave-fragmentized microparticles not in the nano-sized regime. These fragments may represent the largest mass fraction, whereby the entire process thus far is only partially regarded.

To gain further insights into the mechanisms of laser fragmentation, experiments with controlled laser fluence are required. In this work, an experimental design will be demonstrated that allows studying mechanisms of laser fragmentation without the drawback of strong laser fluence deviation. This will be shown and discussed in the experimental section, where comparison to the state of the art is also explored. In general, interaction of laser light with metallic (plasmonic) and dielectric materials has to be differentiated: the former has been studied

intensely using gold nanoparticles and several mechanisms depending on applied laser parameters have been described [Werner2011], [Werner2011a], [Katayama2014], [Hashimoto2012], [Link1999c], whereas for the latter only few theoretical and practical studies have proposed mechanisms for the laser-induced fragmentation [Zhigilei1998], [Cai1998]. Due to the difference in their electronic structure, metals and metal oxides are proposed to interact differently to laser irradiation. Therefore, the interaction of plasmonic and non-plasmonic materials will be presented in two different sections.

Precise studies determining the fluence thresholds for non-metallic particles do not exist. Heise et al. reported a strong dependence of the substrate for the ablation threshold of ZnO layers (around 1 µm) [Heise2011]. In case of a transparent glass substrate, they determined the ablation threshold to be around 4.5 (±0.5) J/cm² for 532 nm wavelength and 10 ps pulse length [Heise2011]. In case of an absorbing substrate, the threshold was found to be around 0.024 (±0.005) J/cm². Risch et al. reported the ablation threshold of 200 nm gallium doped ZnO layers on glass substrates. They found for 532 nm thresholds of around 1.1 J/cm² or 0.84 J/cm² for rear side laser irradiation [Risch2011]. The deviation to the findings of Heise et al. might arise from the doping of ZnO with gallium.

For plasmonic nanoparticles, Pyatenko et al. simulated the fluence thresholds for different laser wavelengths of nanosecond lasers (fundamental, 2nd harmonic and 3rd harmonic of Nd:YAG lasers) in dependence of the particle size [Pyatenko2013]. This valuable review covers silver, gold, copper, platinum and palladium nanoparticles and provides comprehensive insights. Together with the mechanistic findings from Hashimoto and co-workers [Hashimoto2012], a detailed understanding of the mechanisms and thresholds can be drawn. The mechanistic understanding of PLFL for non-metallic and metallic particles will be discussed in 2.5.1 and 2.5.2, respectively.

2.5.1 Interaction of laser light with non-metallic particles

At present, only little is known about the fragmentation mechanisms for ceramic or metal oxide particles interacting with intense laser light. Theoretical studies investigating the interaction of inorganic and organic particles were reported in 1997 and 1999, respectively [Cai1998], [Zhigilei1998], whereby their simulations

revealed a particle disruption from the inside. Studies of Yeh et al. showed the partial reduction of CuO to elemental Cu nanoparticles in isopropanol [Yeh1998] [Yeh1999], thus changing the nanoparticle composition by reduction of copper-(II)-oxide microparticles partially to elemental copper nanoparticles. Interestingly, they obtained higher colloidal stability of their elemental copper nanoparticles than reported for chemically synthetized [Yeh1999]. In a subsequent study, Schaumberg et al. reported the formation of elemental copper nanoparticles from copper compounds such as CuO, Cu_3N and Cu_2C_2 in ethyl acetate [Schaumberg2014]. The results for copper nanoparticle formation from CuO of these practical studies indicate a material vaporization and recomposition under reductive conditions. Thus, the term ablation from particles is used by some researchers as the mechanism might be similar to PLAL. Considering the studies mentioned, it is obvious that there should be different mechanisms for particle size reduction, such as a disruption which might be driven by shock waves [Cai1998], [Wagener2012] and a material vaporization similar to PLAL. However, reports demonstrating that both of these mechanisms simultaneously occur, do not exist, to my best knowledge.

Beside these findings, fragmentation studies of organic materials showed that especially for ultra-short laser pulses (femtosecond) the particle decomposition is less significant than for nanosecond pulses [Sylvestre2011]. The variation of laser power for nanosecond and femtosecond PLFL revealed smaller particles with higher laser power as well as a higher degree of degradation of the pharmaceutical substrate. This might already be an indication of the two mechanisms simultaneously occurring for organic particles, namely disruption or fragmentation and vaporization. Extensive studies of fragmentation of organic microparticles are reported by the Asahi group [Tamaki2000], [Tamaki2002], [Sugiyama2006], [Jeon2007], [Asahi2008], [Sygiyama2011], who showed the (partial) preservation of organic particle composition after laser irradiation with nanosecond lasers using a variety of organic materials and solvents. In contrast to metallic and organic materials, mechanistic understanding of laser fragmentation for inorganic and non-metallic particles is poor despite these materials being intensively investigated by laser ablation, already focusing of breaking the limit of gram per hour yield [Sajti2010], [Intartaglia2014], [Wagener2010]. This limitation for PLAL results from shielding effects of the plasma-induced cavitation bubble hampering the subsequent laser pulse to reach the target. To avoid this and achieve a high productivity, high scanning velocities and repetition rates are necessary [Wagener2010]. Thus, PLFL of these materials will also hold interest because laser fragmentation might be more efficient than

PLAL. This assumption can be driven from a higher degree of freedom that suspended particles have compared to a bulky target material. Studies for PLAL of thin wires have shown an improved productivity [Messina2013]. For this purpose, one possible explanation is the improved specific surface area that can be reached by the focused laser beam. If the laser beam is focused at the tip of a thin metal wire, the nanoparticles can be released from the cavitation bubble, which can expand in almost all directions into the liquid. The only confinement is the longitudinal elongation of the wire. This elongation does not exist for particles completely covered by the laser beam. Note that there are no studies or evidence of cavitation bubbles reducing the process effectivity of PLFL. Moreover, studies reporting the nanoparticle yield per pulse from PLFL remain absent. A study by Jang et al. investigated the shock-wave formation at Cu microparticles in gas phase and determined velocities from 1000-4000 m/s and lower thresholds for ablation compared to a Cu bulk target [Jang2004]. This is another good indication for a possibly higher yield of PLFL compared to PLAL.

Considering the aforementioned investigations on laser fragmentation, it is obvious that the influence of pulse length [Sylvestre2011], laser wavelength, applied laser fluence [Sylvestre2011] and educt particle properties does not reveal a comprehensive laser fragmentation model for non-metallic particles at present. Furthermore, it is unclear when particle composition will be preserved for nanoparticles and when the composition changes. Preservation of material composition as well as decomposition or change in stoichiometry has been shown for nanosecond lasers, as discussed in the aforementioned studies by Yeh et al. [Yeh1998], [Yeh1999], Sylvestre et al. [Sylvestre2011] and Tamaki et al. [Tamaki2000], [Tamaki2002]. Own preliminary investigations on zinc oxide particles showed that nanoparticle formation efficiency could be increased by pre-treatment of the microparticles in a stirred media mill, resulting in the activation of the microparticles fabricating spherical nanoparticles (Fig. 5) [Wagener2012]. From these findings, a contribution of a shock wave and laser-induced plasma at particles' surface for PLFL contribution was assumed. Considering the state of the art, there is a demand to understand the contribution of laser fluence to PLFL for non-metallic particles, which will be addressed accordingly in chapters 4.1, 4.2, and 4.5 of the experimental sections.

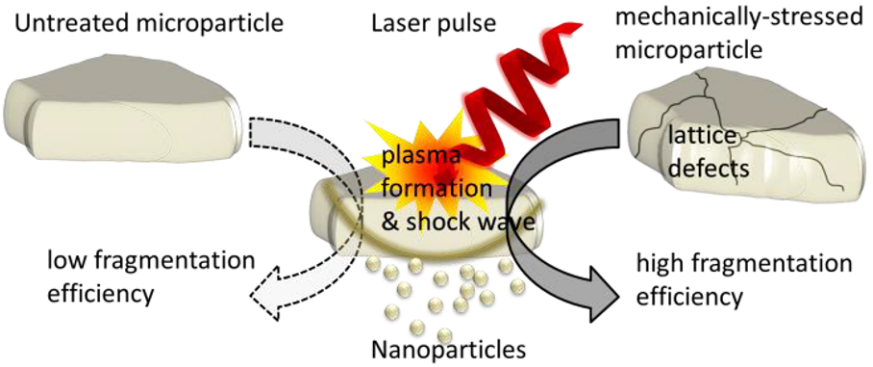

Figure 5: Schematic illustration of nanoparticle release from microparticles found for zinc oxide taken with permission from [Wagener2012]

2.5.2 Interaction of laser light with metallic particles

Some of the earliest studies on laser fragmentation of colloidal metallic nanoparticles date back to 1999, when Link and El Sayed reported that the second harmonic of Nd:YAG lasers fits well to surface plasmon resonance of gold nanoparticles [Link1999a], [Link1999b]. Their experiments also covered investigations of laser pulse length and fluence [Link1999c]. They addressed a wide regime of pulse length and laser fluence at the same time. Link et al. could show that laser treatment of nanorods results in sequential formation of spherical particles for different fluences and pulse lengths at 800 nm wavelength. This wavelength corresponds to the 2nd plamon peak of the nanorods used and thus was selective for rods' excitation. Due to a stepwise transformation from Au rods to spheres, these investigations might be considered as a first approach and strategy enabling energy dose balancing. Following these reports, a variety of plasmonic materials were investigated for their response to laser irradiation [Amendola2009], showing that laser parameters such as laser fluence can be correlated to obtained nanoparticle properties such as diameter. Mafuné and Kondow reported about small platinum nanoparticles stabilized by SDS generated with 355 nm laser irradiation [Mafuné2004] as well as gold nanoparticles stabilized with SDS for PLFL with 532 nm laser wavelength [Mafuné2001]. This shows that besides the laser wavelength and fluence, the

surfactant concentration also has a crucial impact on received nanoparticle sizes. The crucial role of surface chemistry in particular oxidation for Au NP produced by PLAL in water was first described by Sylvestre et al. [Sylvestre2004], [Sylvestre2004a].

Alloy formation by laser irradiation of mixed Ag-Au particle microparticle suspensions was already reported in 2003 by Zhang et al. [Zhang2003], who adapted the idea of alloying nanoparticles by laser irradiation from Chen et al. [Chen2001]. These studies mentioned the advantages of using educt microparticles for alloy formation compared to alloy formation from colloidal mixtures of nanoparticles, although PLAL might be considered as the method of choice for alloy formation to avoid educt-product mixing. Regarding this issue, Jakobi et al. reported the preservation of stoichiometry after ablation [Jakobi2011] and Neumeister et al. characterized crystalline and homogenous ultra-structures of the produced alloy NPs [Neumeister2014]. Furthermore, Neumeister et al. cross-checked the alloy formation by PLAL with post-irradiation of colloidal mixtures from Au and Ag nanoparticles, revealing no alloy formation.

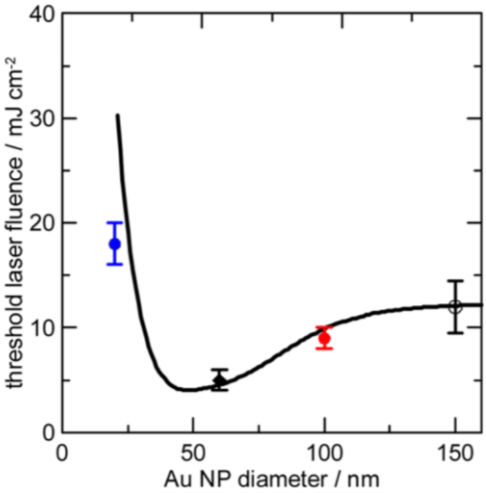

Figure 6: Bubble formation threshold for different gold nanoparticle diameter excited with 15 ps pulses and 355 nm wavelength [Katayama2014]; Reprinted (adapted) with permission from [Katayama2014]; Copyright (2014) American Chemical Society

The interaction of particles with the incident laser light strongly depends on particles extinction cross section and their absorption efficiency at the laser wavelength used [Link1999a]. Katayama et al. investigated the threshold for the formation of a bubble that is generated around plasmonic particles by laser irradiation in dependence of nanoparticle size. Figure 6 depicts the curve showing this fluence threshold for different particle diameter using an excitation pulse length of 15 ps [Katayama2014].

The findings for bubble formation threshold (Fig. 6) correlate with experimental findings for fragmentation thresholds from Cavicchi et al., who used 532 nm wavelength and 7 ns pulse length for the change of gold nanoparticle sizes for different laser fluences and educt particle diameter [Cavicchi2013]. Therefore, independent of pulse length and wavelength, particle sizes between 30 to 100 nm exhibit most efficient laser light absorption and lowest bubble formation thresholds [Katayama2014], [Pyatenko2013] [Gökce2015a]. In particular, studies by Cavicchi et al. revealed the lowest fragmentation threshold for 60 nm Au NP comparing 10nm, 20nm, 30 nm, 60 nm and 100 nm Au NP sizes [Cavicchi2013], indicating a correlation between bubble formation threshold and the fragmentation threshold.

Due to this reason, Au NP particles with a size range close to the minimum of the threshold laser fluence are most difficult to obtain from laser irradiation. Although this size fraction is often obtained as a second mode after PLAL (depending on laser parameters) [Kabashin2003], this particle size regime can hardly be synthesized by further laser irradiation of the colloid, given that particles in this size regime will interact at the lowest laser fluence threshold and thus be first transformed into different sizes.

Therefore, accessing gold nanoparticles with 50 nm in diameter that have the advantage of high purity as known for laser-generated particles will be challenging. One possibility is to separate the 50 nm particles, formed by PLAL without size quenching by fractional centrifugation [Bonaccorso2013]. On the other hand, Au NP in the size regime of 50 nm are a perfect educt for fundamental PLFL studies, as shown by Hashimoto et al. [Hashimoto2012].

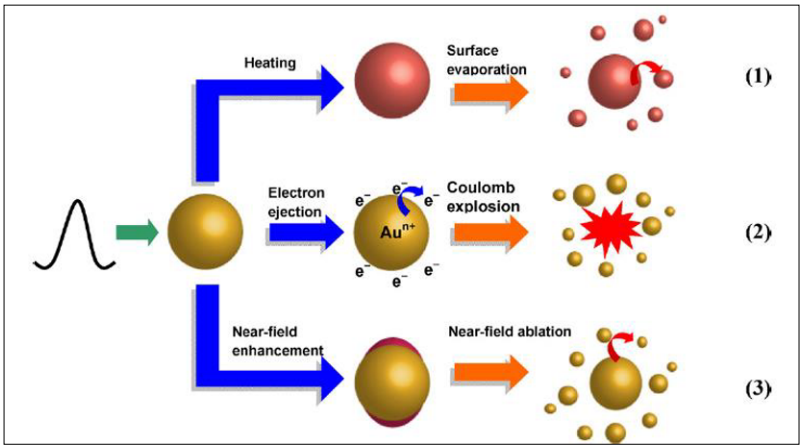

Figure 7: Mechanisms for fragmentation of gold nanoparticles excited by pulsed lasers taken with permission from [Hashimoto2012]

Werner et al. showed that monodisperse gold nanoparticles can be generated with high reproducibility using high pressure chambers for laser irradiation of 100 nm gold and silver nanoparticles [Werner2013]. Hashimoto and co-workers proposed a general fragmentation model for the interaction of laser light with plasmonic particles, as shown in Figure 7. They distinguished three possible mechanisms for change of plasmonic particles size. One is release of small particles by vaporization of particles' surface due to sufficient heating of the particle. Another model is the coulomb explosion, occurring when several electrons are effectively dislocated from their atomic partner in a small area. This results in the atoms' strong repulsion to each other and causes disruption of the atomic structure, the so-called coulomb explosion. As proposed, the effective excitation of the surface plasmons can also result in a release of nanoparticles. This near-field ablation mechanism demands laser wavelengths close to the surface plasmons' wavelength. The model has recently been refined by Strasser et al., correlating particle temperature with the change in size and shape [Strasser2014]. Nonetheless, independent of the occurring mechanism, if particles are fragmentized they will undergo subsequent ripening and thus particle sizes will increase after fragmentation. To avoid this, one possibility is size quenching by organic ligands, although this will cover the particle surface, which might hinder later applications. Hence, investigations are required to address how the size limit of around 4 nm can be overcome, thus fabricating ultra-small and ligand-free gold nanoparticles.

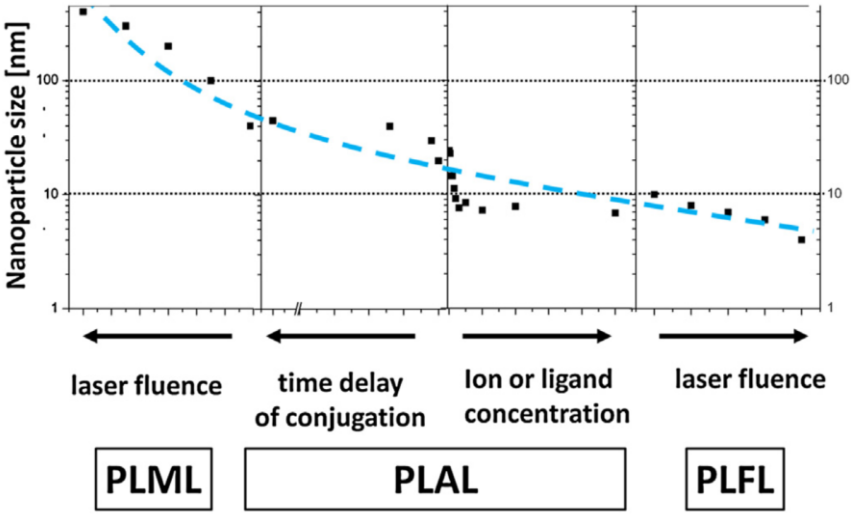

Figure 8: Achievable sizes for laser-generated gold nanoparticles by different strategies (taken with permission from [Asahi2015]) adapted from [Rehbock2014]

These particles hold particular interest as below 5 nm particle diameter relevant catalytic activity starts [Haruta1997] and the origin of fluorescence on gold atom clusters (<3 nm) remains under debate [Goldys2012].

A recent review from Rehbock et al. summarizes the possibilities of size control for pure metal and metal alloy nanoparticles using pulsed laser irradiation [Rehbock2014]. This review demonstrates that a wide size range from a few hundreds of nanometers down to around 4 nm can be addressed by treatment with pulsed lasers.

2.6 Fundamentals of pulsed laser melting in liquids

Pulsed laser melting in liquids (PLML) is a technique to generate spherical particles in the sub-micrometer range by laser irradiation. In contrast to laser fragmentation where educt particle size is reduced, laser melting causes particle fusion and reshaping to sub-micrometer spheres. First reported and established

by Naoto Koshizaki and co-workers [Wang2010, Ishikawa2007], this technique is gaining increasingly attention, becoming an emerging research field. PLML enables changing particles' structure (such as size and shape) and the chemical composition, both of which depend on the applied laser fluence. To provide a comprehensive overview of the current state of the art, this chapter is divided into the influence of PLML on particle chemistry and the influence of PLML on particle size and shape.

Influence of PLML on particle chemistry

Following their pioneering studies Wang et al. investigated different materials for PLML, such as zinc oxide sub-micrometer spheres (SMS) [Wang2011], and Ishikawa et al. reported about boron carbide SMS by laser irradiation of boron particles in ethyl acetate [Ishikawa2007]. For this, they assumed a mechanism [Ishikawa2010] proposing that in the region of the focal point the boron is transferred into boron carbide and in lower fluence regimes the boron carbide particles fusion to SMS. They suggest a laser-induced development of a carbon layer onto educts' (boron nanoparticles) surface prior to a followed laser melting. During their experiments, they focused the laser beam into the colloidal suspension and differentiated between two regimes. Close to the focal point, the carbonization of boron nanoparticles is assumed and in the regions with lower laser fluences melting is proposed.

Detailed experimental studies from Wang et al. showed that CuO nanoparticles can be partially chemically reduced to metallic SMS. The starting of PLML for CuO was found to be at laser fluence thresholds of around 33 mJ/cm² (10 ns, 355 nm) [Wang2012]. They found laser fluences between 17 mJ/cm² and 33 mJ/cm² as onset for PLML. Above the melting onset fluence and below ~80 mJ/cm², no elemental Cu could be observed, but a gradual change of the elemental composition from CuO to Cu_2O by increasing fluence. Further increasing the laser fluence, above ~80 mJ/cm² results in the formation of elemental Cu with a composition ratio up ~40% of elemental Cu for 150 mJ/cm².

In 2013, Swiatkowska-Warkocka et al. reported about bimetallic SMS by fusion of gold and copper oxide nanoparticles [Swiatkowska-Warkocka2013]. They showed that pulsed laser melting in ethanol of Au-NP and copper oxide nanoparticles can generate bimetallic and crystalline SMS. Remarkably, they could synthesize alloy SMS with a composition that shows phase separation in phase diagram.

Another interesting approach was introduced by Li et al. [Li2011a], who reduced Ag_2O to Ag SMS by PLML.

Tsuji et al. recently reported about the influence of surface chemistry for PLML of Au to form SMS [Tsuji2015]. In case of sufficient particle stabilization, the fusion is hindered due to a controlled repulsive surface charge.

Influence of PLML on particle size and shape

Wang et al. found besides the gradual reduction from CuO to Cu that for increasing laser fluence the particle diameter of CuO SMS (or the partially reduced CuO SMS) gradually increases [Wang2012]. Up to 150 mJ/cm², they received smooth SMS particle surfaces, whereas for laser fluences at 150 mJ/cm² particles appear to be rough, indicating that particle fragmentation starts [Rehbock2014a].

Wang et al. also investigated PLML onset for zinc oxide particles, finding it to be between 33 mJ/cm² and 67 mJ/cm², which is also in the regime for our findings [Wang2011]. Later investigations by Wang et al. focused on silver nanoparticles that were transformed into SMS by PLML [Wang2013]. Tsuji et al. investigated PLML of Au NP for laser fluences from 40 mJ/cm² and 100 mJ/cm² [Tsuji2013]. Likewise, Wang et al. found for copper SMS that the size of Au SMS increases with increasing laser fluence. Beside this, Tsuji et al. found that salt-induced educt particle agglomeration is preferential for sufficient PLML of Au NP with 532 nm laser wavelength.

Ceramic materials such as zirconia SMS or hollowed titanium dioxide SMS are reported by Li et al. [Li2012] and Wang et al. [Wang2011a], respectively. Additionally Li et al. reported about silicon SMS [Li2011b].

The current state of PLML shows that particles' chemistry and size are influenced by the laser fluence applied during PLML. Thus, PLML is not only particle melting, fusion and re-solidification as spheres, but it can be. This part of the mechanistic understanding is illustrated in Figure 9, taken from Higashi et al. [Higashi2013].

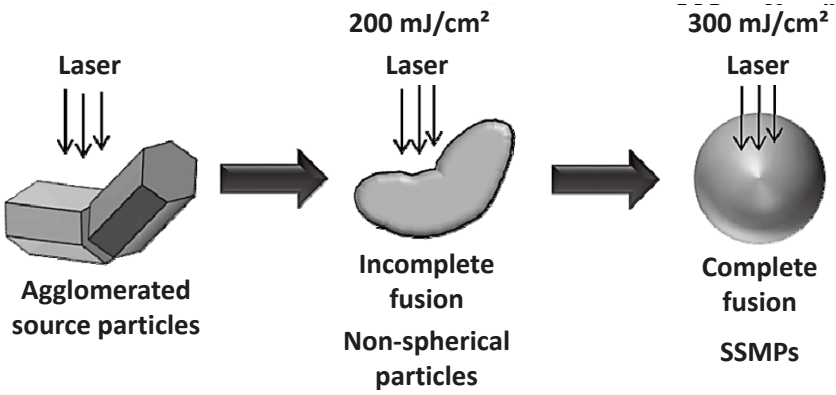

Figure 9: Proposed mechanism for PLML of zinc oxide particles [Higashi2013]

Although exact formation mechanisms are not yet fully understood, early reports on possible applications are available. One possible application has been shown by Fujiwara et al., who used ZnO SMS generated by PLML as a light-emitting laser source [Fujiwara2013]. They added polystyrene particles (900 nm with green fluorescence properties) to a ZnO SMS (synthesized by PLML) film as point defects and showed that the emission threshold for lasing decreases. They describe the lasing effects being improved by PLML of ZnO.

Another recently demonstrated application is the use of SMS as additive for lubricant oils to reduce friction. Hu et al. demonstrated the impact of ZnO, TiO_2 and CuO SMS on reduction of friction coefficients in lubricant oils [Hu2012]. They showed that the friction coefficient decreases if SMS are added to oil, whereas the presence of ZnO educt microparticles in the oil which were not transferred into SMS by PLML showed an increase in the friction coefficient. Liu et al. recently reported about monodisperse Au SMS applied sufficiently for an improved surface enhanced Raman scattering [Liu2015].

To summarize the current state of the art for PLML for sub-micrometer spheres formation, it can be stated that a comprehensive mechanistic understanding of SMS formation is lacking.

Especially the possibility to generate hybrid material compositions and the change in particles' chemical composition holds particular interest and should allow studying the mechanisms responsible for SMS formation. For this purpose,

it will be necessary to correlate the applied laser fluence for PLML with the change of particles' elemental composition.

In contrast to laser fragmentation in liquids, detailed studies for PLML thresholds exist, owing to the lower fluences demanded to cause sufficient particle melting. Therefore, unfocused laser beams can be used. In case of focusing, the precise control of applied fluence becomes difficult, possibly reflecting the reason for a lack of sufficient data determining the PLML regime at higher laser fluences. Here, the experimental design developed within this work might come into play to address precisely the high laser fluence regimes, e.g. for precise control of chemistry and melting conditions.

http://www.springer.com/978-3-658-14170-7

Laser Fragmentation and Melting of Particles

Lau, M.

2016, XX, 258 p. 118 illus., Softcover
ISBN: 978-3-658-14170-7